JOURNAL OF Materials CHEMISTRY

Atomistic simulation methodologies for modelling the nucleation, growth and structure of interfaces

Dean C. Sayle,[a] C. Richard A. Catlow,[b] John H. Harding,[c] Matthew J. F. Healy,[d] S. Andrada Maicaneanu,[a] Stephen C. Parker,[e] Ben Slater[b] and Graeme W. Watson[f]

[a]*Department of Environmental and Ordnance Systems, Cranfield University, Royal Military College of Science, Shrivenham, Swindon, UK SN6 8LA. E-mail: sayle@rmcs.cranfield.ac.uk*
[b]*The Royal Institution of Great Britain, 21 Albemarle Street, London, UK W1X 4BS*
[c]*Materials Research Centre, Department of Physics and Astronomy, University College London, Gower Street, London, UK WC1E 6BT*
[d]*Department of Materials and Medical Sciences, Cranfield University, Royal Military College of Science, Shrivenham, Swindon, UK SN6 8LA*
[e]*School of Chemistry, University of Bath, Claverton Down, Bath, Avon, UK BA2 7AY*
[f]*Department of Chemistry, Trinity College, Dublin 2, Ireland*

Received 9th February 2000, Accepted 20th March 2000
Published on the Web 9th May 2000

There have been many studies applying atomistic simulation techniques to investigate the structure and energetics of surfaces and interfaces. Almost all start by defining the basic structure of the interface, which is then simulated by static or dynamical methods. A different approach is adopted here, where we allow interfacial structures to evolve during the course of the simulation. In particular, three atomistic simulation methodologies for constructing models for thin film interfaces have been developed, including 'atom deposition', where the thin film is 'grown' by sequentially depositing atoms onto a support material to obtain information on nucleation and growth mechanisms; 'layer-by-layer' growth, where monatomic layers of a material are successively deposited on top of a substrate surface; and finally, 'cube-on-cube' whereby the whole of the thin film is placed directly on top of the substrate, before dynamical simulation and energy minimisation. The methodologies developed in this study provide a basis for simulating the nucleation, growth and structure of interface systems ranging from small supported clusters to monolayer and multilayer thin film interfaces. In addition, the layer-by-layer methodology is ideally suited to explore the critical thickness of thin films. We illustrate these techniques with studies on systems with large negative misfits. The calculations suggest that the thin films (initially constrained under tension due to the misfit) relax back to their natural lattice parameter resulting in the formation of surface cracks and island formation. The cube-on-cube methodology was then applied to the SrO/MgO system, which has a large (+20%) positive misfit. For this system, the SrO thin film underwent an amorphous transition which, under prolonged dynamical simulation, recrystallised revealing misfit-induced structural modifications, including screw-edge dislocations and low angle lattice rotations.

Introduction

Many material properties are governed by the presence of interfaces. For example, epitaxial growth of a material onto a (lattice mismatched) substrate surface will result in structural modifications such as dislocations, grain-boundaries, cracks and fractures,[1] which may influence, for example, the mechanical,[2] catalytic[3] and electronic[4] properties of the material. Moreover, whereas certain structural modifications may enhance the desired material properties, others, such as dislocations within supported superconductors, may prove deleterious. The structural characterisation of interfaces and the relationship of structure to properties are central to materials science and engineering.

Experimental techniques, such as HREM and X-ray diffraction,[1] have provided valuable atomistic models of interfaces and grain-boundaries. Indeed, such is the resolution of contemporary microscopy techniques that detailed structural models of interfaces at the atomistic level have been proposed.[5–7] For example, Ernst *et al.* have been able to characterise fully the core structure of an edge dislocation within the $SrZrO_3/SrTiO_3$ interface.[8] However, notwithstanding the tremendous advances made, experimental work in this area remains very difficult. Atomistic computer simulation techniques are ideally placed to complement experimental work in the area of interfacial structural characterisation. Indeed, simulation can help rationalise the detailed atomistic structures and properties of interface systems[9] including, for example, growth and nucleation,[10,11] supported clusters,[12] epitaxy,[13–17] buffer layers,[10,18] elastic and mechanical properties,[2] dislocations,[19–25] critical thicknesses[26] and chemical properties.[27,28]

In this study, we present three methodologies for modelling interfaces ranging from the growth, nucleation and structure of supported clusters to monolayer and multilayer thin films. We then illustrate these techniques using a range of simple model oxide–oxide interface systems.

Simulation methods

The MARVIN code[29] was used to perform both the energy minimisation and dynamical simulations reported in this paper. The code considers the crystal as a stack of ions periodic in two dimensions, where the stack consists of a whole number of repeating units in the direction normal to the interface. The stack is subdivided into two regions, as depicted in Fig. 1: a region I, where all the ions are allowed to relax explicitly, and a region II, where the ions are all held fixed relative to each other. Region II is included to ensure that the long-range effects of the ions in the bulk of the crystal on the surface region are correctly

DOI: 10.1039/b001094o

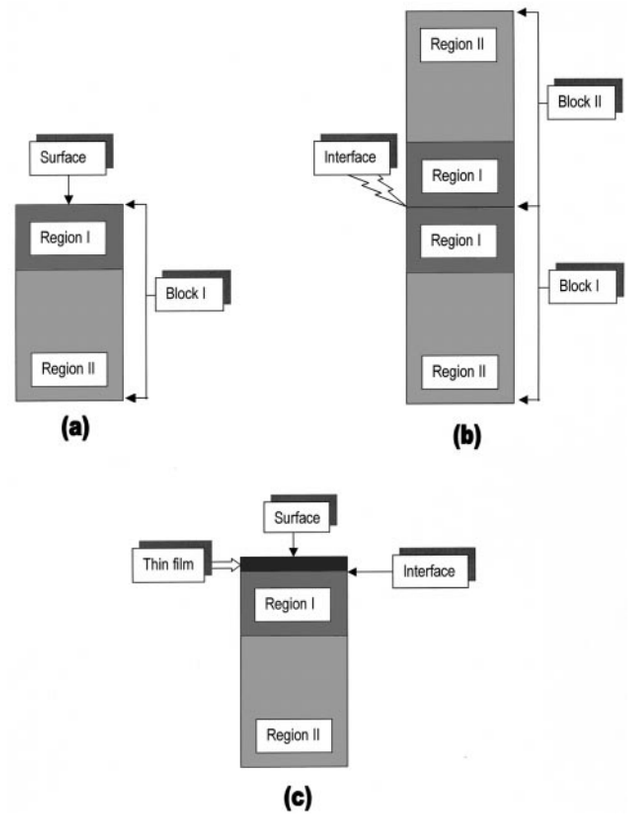

Fig. 1 Schematic depicting the methodology employed within the two-dimensional surface code MARVIN.

represented. The top of region I is the free surface, onto which ions comprising the thin film are deposited, thus creating the interface. To reduce the computational cost, the thickness of regions I and II for the support was one and three unit cells respectively.

The reliability and quality of the simulation is intimately dependent upon the potential models describing the materials under investigation. The interionic potentials used in this present study are, as is normally the case for metal oxides, based on the Born model of the ionic solid in which the ions interact *via* long-range Coulombic interactions and short-range, parameterised interactions. Potential parameters for all the ions considered in this study were taken from Lewis and Catlow.[30] A rigid ion model was used to reduce the computational expense.

Surface calculations can predict the relative stability of surfaces and interfaces *via* the surface energy, which is defined as the energy required to create the surface, per unit area, from the bulk material. The surface energy is given by:

$$\gamma_{\text{surface}} = E_{\text{surface}} - \frac{1}{2}E_{\text{bulk}}/\text{Area} \quad (1)$$

and requires two calculations to be performed, a surface calculation (E_{surface}), with one block [Fig. 1(a)] and a bulk calculation (E_{bulk}) with two blocks [Fig. 1(b)]. For supported thin films we define a thin film (TF) interface energy as:

$$\gamma_{\text{TF interface}} = [E_{\text{TF interface}} - \frac{1}{2}E_{\text{bulk}} - n(E_{\text{TF}})]/\text{Area} \quad (2)$$

where $E_{\text{TF interface}}$ is the total energy of the interface [Fig. 1(c)], E_{bulk}, the bulk energy of the substrate [Fig. 1(b)], E_{TF}, the standard three dimensional periodic bulk energy for the supported thin film material per formulation unit and n is the number of formula units of the supported thin film.

The thin film interfaces were constructed in three ways; Fig. 2 illustrates the procedures.

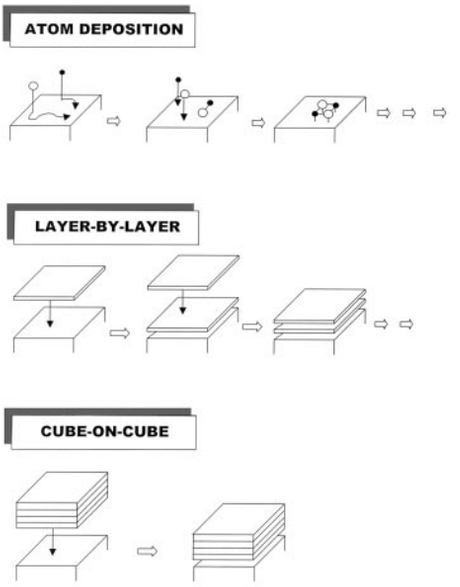

Fig. 2 Schematic depicting the three simulation methodologies employed in this study.

Atom deposition

The interface was generated by successively depositing individual ions onto the substrate surface until a film of the required thickness was achieved. A driver program was written to automate the deposition process and was used in conjunction with the MARVIN code, which performed the minimisation and dynamical simulations. The program introduces the ions comprising the thin film at random positions above the substrate surface within the bounds of the surface repeat unit, and moves them vertically towards the surface until they are within 2.5 Å of the current surface. Energy minimisation and/or dynamical simulation is then applied to the whole system. The process was repeated until the required thin film thickness was reached. Since dynamical simulation is applied to the system after each deposition step, the approach is computationally expensive and therefore the use of large simulation cells and the creation of films of significant thickness may not be possible. Conversely, the merits of this approach include the investigation of epitaxial growth mechanisms, nucleation sites and the generation of clusters at sub-monolayer deposition levels.

Layer-by-layer epitaxial growth

Here the interface is created *via* the sequential deposition of monolayers onto the substrate surface as in the attachment energy model of crystal growth.[29] A monolayer is first placed on top of the substrate surface and dynamical simulation followed by energy minimisation applied to the system, after which a further monolayer is 'deposited' and again dynamical simulation and energy minimisation is performed. The cycle is repeated until the desired film thickness is reached. Since the dynamical simulation is applied after the addition of each monolayer as opposed to each atom, the procedure is less computationally expensive and therefore larger cells and thicker films may be simulated.

Cube-on-cube construction

The interface is generated by placing the whole of the thin film directly onto the substrate surface before the dynamical simulation and energy minimisation. Since only a single dynamical simulation is performed, a much larger simulation cell may be considered, providing more structural detail on the formation of misfit-induced defects, such as dislocations, lattice

slip and twist boundaries. Indeed, since such defects may be larger than the simulation cells employed in either the atom deposition or layer-by-layer approach, the cube-on-cube methodology offers a viable approach for elucidating their structure. Conversely, information regarding growth or nucleation mechanisms is sacrificed within this simulation regime.

In contrast to the atom-deposition methodology, the initial configuration of the thin film with respect to the underlying support must be given for both the layer-by-layer and cube-on-cube methodologies. In this study, for each of the systems investigated, an 'on-top' configuration was chosen, whereby the cations and anions of the thin film were constrained to lie directly above their respective counterions in the underlying support. Alternative starting configurations may be considered, in which the 'epitaxial' relationship between the thin film and the support material is chosen to generate geometrically lattice matched starting configurations with lower associated lattice misfits. Such configurations, and their influence on the final interfacial structure, will be addressed in a future study.

Systems with a negative misfit

We now explore the application of all three methodologies to interfaces where the supported thin film has a smaller lattice parameter compared with the substrate. In particular we consider the SrO/BaO(001) and MgO/CaO(001) interface systems.

Atom deposition; SrO/BaO(001)

The lattice parameters for SrO and BaO are 5.16 and 5.54 Å respectively, which represents a −6.8% lattice misfit for the system. To construct the SrO/BaO(001) interface, Sr and O ions were successively deposited onto a (10×10) BaO substrate, which corresponds to 10 atoms or 5 BaO repeat units for each side of the periodic simulation cell. Each lattice plane of the BaO(001) support surface within the simulation cell therefore comprises 100 atoms and has a surface/interfacial area of 760 $Å^2$.

After the deposition of 21 SrO species [Fig. 3(a)], the SrO was observed to form clusters on the BaO support, with the Sr and O species lying almost directly above their respective counter-ions in the support. Calculated SrO bond distances range from *ca.* 2.3 Å at the cluster edge to 2.6 Å at its centre with an interfacial separation of *ca.* 2.6 Å. The natural Sr–O bond distance is 2.58 Å. Directly below the SrO cluster, Ba–O bond distances range from *ca.* 2.6 to 3.0 Å, which demonstrates a significant perturbation of the underlying support material; the natural Ba–O bond distance is 2.76 Å. Upon further deposition of Sr and O species, cluster growth was observed (as opposed to the formation of isolated and dispersed Sr and O species), which suggests that the clusters provide energetically favourable nucleation sites for the adsorption of Sr and O species compared with a 'clean' BaO surface in accord with previous studies.[12] Inspection of the system after further deposition of SrO species revealed the evolution of a second SrO layer [Fig. 3(b)].

Finally, after 250 SrO species had been deposited (five

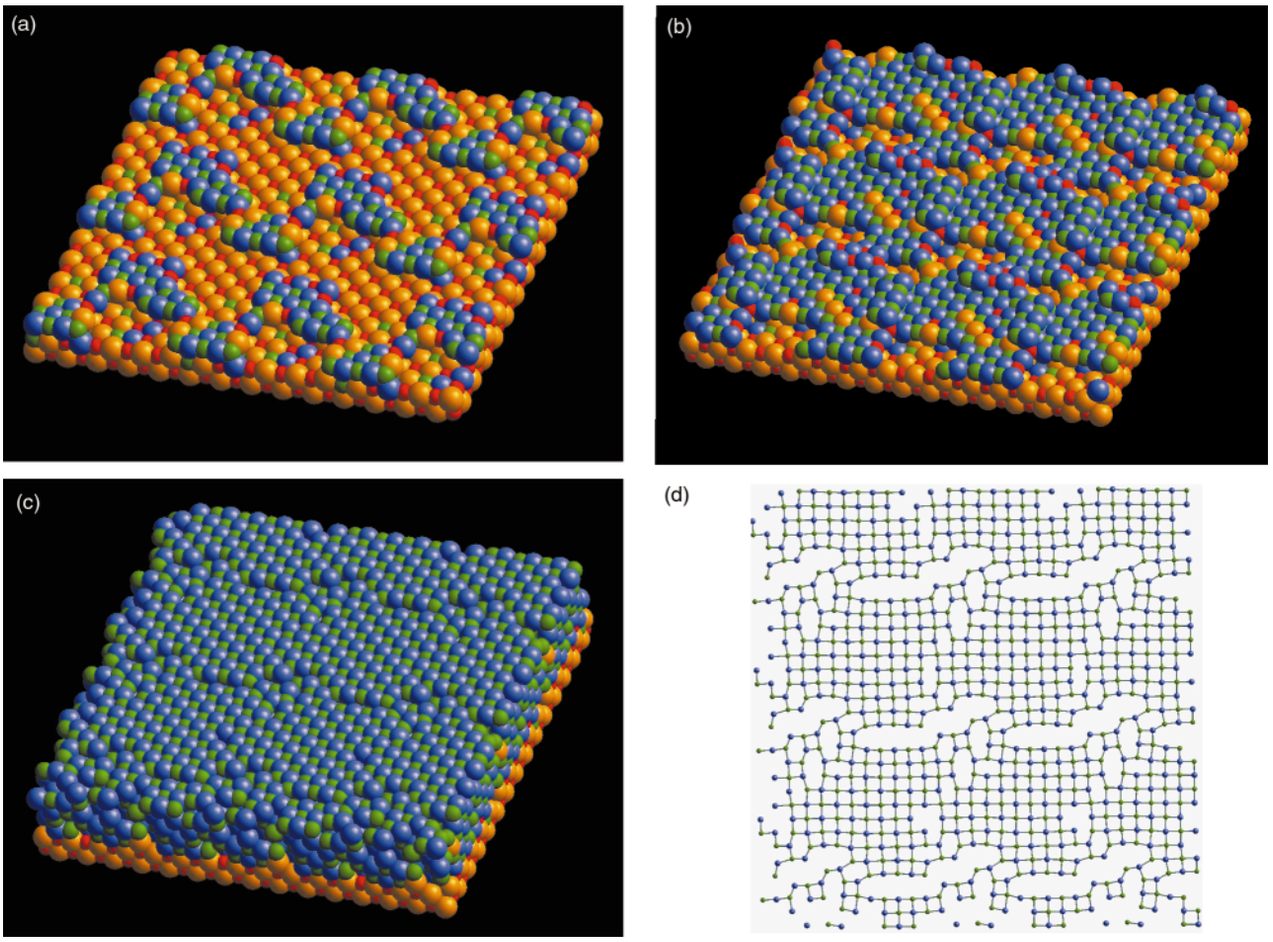

Fig. 3 Representation of the SrO/BaO (001) (10×10) system after the deposition of (a) 21 SrO species; (b) 50 SrO species; (c) 250 SrO species onto the BaO (001) surface; (d) ball and stick representation of the SrO surface layer depicting the cracks. Barium is coloured orange, oxygen (BaO) is red, strontium is blue and oxygen (SrO), green.

'monolayers'), the structure of the SrO ultra thin film could be described as atomically flat and coherent. The Sr and O species maintain an 'on-top' configuration with respect to the BaO support [Fig. 3(c)] with the Sr and O species lying directly above their respective counterions. However, close inspection of the SrO surface layer revealed small fissures or 'cracks' in the surface, which initiate from SrO layer three and increase in size through layers four and five (SrO surface). The maximum Sr–O bond distances (within the cracks) were calculated to be 3.45, 4.12 and 5.04 Å, in layers three, four and five respectively. Fig. 3(d) shows the SrO surface (layer five) depicting more clearly the complex structure of the crack. Radial distribution functions (RDF) were also calculated for each of the SrO layers and revealed the average Sr–O bond distances to be 2.59 (SrO surface), 2.66, 2.72, 2.75, 2.76 (interface) and 2.76 Å for the BaO interfacial plane, which suggests that the SrO relaxes back to its natural lattice parameter further from the interface initiating crack formation. At the interfacial plane the strain energy associated with the 'on-top' configuration is, in part, compensated by the energetically favourable cation–anion interactions across the interfacial plane. Conversely, the strain energy cannot be recovered for SrO planes further from the interface, and therefore the SrO relaxes back to its natural lattice parameter leading to the formation of surface cracks.

Close inspection of Fig. 3(a) and (b) reveals that barium and oxygen ions migrate out of the support during the simulation to fill lattice positions within the SrO cluster. The resulting vacancies within the support are subsequently filled by the Sr,O atoms deposited. An additional calculation was performed in which all the Ba and Sr ions that had migrated (into the SrO thin film and BaO support, respectively) were 'exchanged'. The total energy of this system was found to be higher (less stable) for all deposition levels considered. We suggest that the interdiffusion of the Ba and Sr, within the SrO clusters and BaO support, respectively, helps to accommodate the lattice misfit thereby stabilising the system. Moreover, since the barium ion is larger compared with strontium, the SrO lattice parameter will be increased when a proportion of the Sr lattice sites are filled with Ba. Conversely, a decrease in the BaO lattice parameter will be observed when Sr occupies Ba lattice sites. The simulation therefore suggests that, for this system, a smooth transition from one lattice parameter (SrO) to another (BaO) is energetically favourable compared with a sharp transition with implications for the design of buffer layers within incommensurate interface systems. A study by Lind *et al.* on the growth of Fe_3O_4/NiO thin films using molecular beam epitaxy revealed interfacial diffusion of the Fe_3O_4 and NiO layers of the order of one or two atomic layers.[31]

Inspection of the interface energies of the SrO/BaO(001) system reveals that the interface becomes less stable with thin film thickness (Table 1). The strain energy associated with maintaining an on-top configuration will be additive for each additional plane and cannot be sustained for thick films. Accordingly, at a particular 'critical thickness',[26,32] the strain energy will destabilise the interface system such that it becomes energetically favourable for the system to facilitate the evolution of structural modifications such as dislocations, which reduce the misfit. However, in addition to the thermodynamic considerations, the kinetic pathways for the occurrence of such structural changes must also be surmountable. In a previous study[11] we have demonstrated that the atom-deposition methodology employed here is capable of addressing both the thermodynamic and kinetic aspects associated with such misfit-induced structural modifications. Furthermore, one must also consider the possibility of whether the structural modifications associated with reducing the strain energy are larger than the simulation cell dimensions, which would inevitably preclude their observation.[18] Therefore, to address this issue, the size of the simulation cell must be increased. Accordingly, in the following section a layer-by-layer approach is considered which is less computationally expensive and consequently larger simulation cells can be considered.

Layer-by-layer epitaxial growth; MgO/CaO(001)

The MgO/CaO(001) system, which is associated with a −13% lattice misfit, was generated by successively depositing MgO monolayers directly on top of a (12×12) CaO(001) support following the procedure described above. The surface/interfacial area for the simulation cell is therefore 828 $Å^2$ and comprises 144 atoms in each plane. The interface energies for 1–6 monolayers deposited are presented in Table 1.

After four MgO layers had been deposited, the MgO thin film displayed small 'cracks' or grooves within the MgO [Fig. 4(a)]. Initially, the MgO is constrained to accommodate the entire lattice misfit, and is therefore under tension. Consequently, to reduce the tensile stress within the MgO, the lattice contracts to its natural lattice parameter resulting in cracks within the MgO thin film. RDF values were calculated for each of the MgO layers and reveal that the average Mg–O bond distances are 2.05 (surface), 2.10, 2.17, 2.25 (interface) and 2.35 Å for the Ca–O interfacial plane. The natural Mg–O and Ca–O bond distances are 2.1 and 2.4 Å respectively.

After the deposition of six layers [Fig. 4(b)], the 'cracks' appear to be capped, which perhaps indicates the start of an edge dislocation. The Burgers vector for the dislocation would be parallel to the surface, which implies that the density of the layer increases with the introduction of the dislocation. In addition, to maintain charge continuity, the 'cap' comprises both Mg and O ions. The resulting thin film structure therefore accommodates surprisingly large channels *ca.* 4.6×5.4 Å

Table 1 Calculated thin film interface energies

System	Thin film interface energy/J m^{-2}	Graphic	System	Thin film interface energy/J m^{-2}	Graphic
SrO/BaO(001) 760 $Å^2$			MgO/CaO(001) 5885 $Å^2$		
21 SrO species	1.00	Fig. 3(a)	4 layers	3.76	Fig. 5
50 (1 layer)	1.23	Fig. 3(b)			
2 layers	1.36		SrO/MgO(001) 3455 $Å^2$		
3 layers	1.67		*ca.* 6–7 layers	3.61	Fig. 6, 7
4 layers	1.79				
5 layers	1.83	Fig. 3(c),(d)	SrO/MgO(011) 3490 $Å^2$		
			ca. 6–7 layers	3.92	Fig. 8, 9, 10
MgO/CaO(001) 827 $Å^2$					
1 layer	2.22		SrO/MgO(14 0 1) 3464 $Å^2$		
2 layers	2.94		*ca.* 6–7 layers	3.67	Fig. 11, 12
3 layers	3.62				
4 layers	3.79	Fig. 4(a)			
5 layers	4.23				
6 layers	4.64	Fig. 4(b–d)			

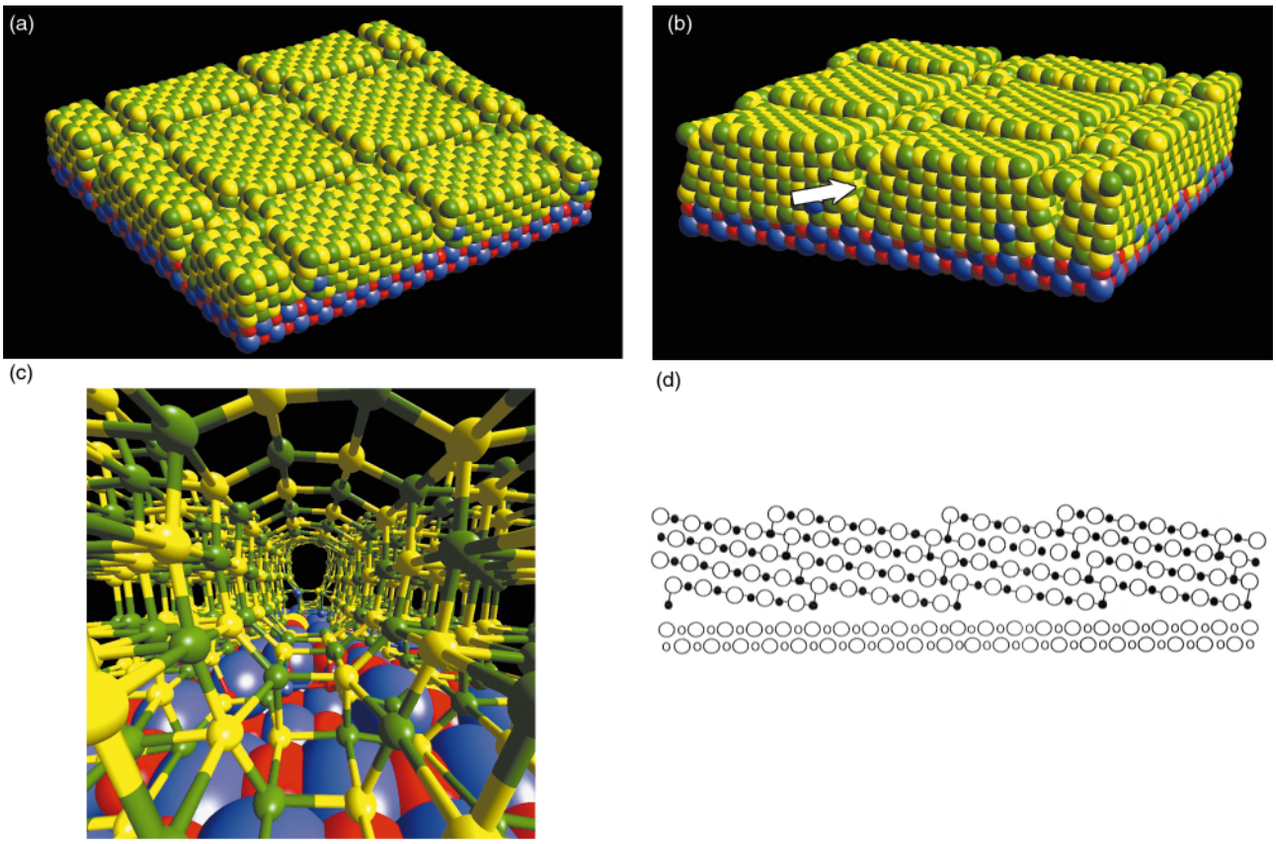

Fig. 4 Structure of the MgO/CaO(001) (12×12) interface after the deposition of (a) four MgO layers; (b) six MgO layers; (c) perspective view looking along the direction of the arrow depicted in Fig. 4(b); (d) schematic of a side view of Fig. 4(b) depicting more clearly the surface steps and similarities with low angle grain-boundaries. Magnesium is coloured yellow, calcium is blue, oxygen (MgO) is green and oxygen (CaO) is red.

diameter, which traverse the length of the MgO thin film. An enlarged, perspective view, looking down one of the channels, is presented in Fig. 4(c). The driving force for such behaviour is again a reduction in the strain energy of the system. For example at the interface, the MgO lies coherent with the CaO support accommodating the full -13% lattice misfit; the stability generated from the perfect alignment of cations and anions across the interface outweighs the energy associated in straining the MgO lattice into coherence. Conversely, further from the interface the MgO relaxes back to its natural lattice parameter at which point there is sufficient space to include an additional 'line' (edge dislocation) of MgO units. We suggest, therefore, that Fig. 4(c) is a view looking down this dislocation core. The lattice misfit can be estimated to be *ca.* $+2\%$ based upon 14 MgO lattice planes of 2.1 Å latticed matched with 12 CaO lattice planes of 2.4 Å [Fig. 4(b)]. Moreover, the calculation suggests that the critical thickness is less than 6 atomic layers for this system.

The 'layer-by-layer' methodology is ideally suited to determine the critical thicknesses of materials with associated lattice misfits of greater than $\pm 1\%$; for smaller lattice misfits the critical thickness is likely to be so high that the number of planes required within the simulation would far exceed the computational resources available.[26]

Further inspection of the structure reveals the presence of steps on the MgO surface [Fig. 4(b),(d)], indicating additional dislocations within the thin film.[33] The dislocation structure can perhaps be better described as a simple tilting (*ca.* 6°) of the MgO thin film with respect to the support, which enables the thin film to accommodate, in part, the lattice misfit. Such structures have been observed in a previous study.[18] The supported thin film exhibits structural similarities to low angle grain boundaries which have been studied extensively both experimentally[1,34,35] and using simulation techniques.[21,22,36–38] However, previous simulation studies on grain-boundaries have involved generating ('artificially') the grain boundary structure before energy minimisation and dynamical simulation by placing the particular surfaces together in the appropriate orientation. In contrast, the structures identified in this present study have 'evolved' under dynamical simulation during the sequential deposition of monolayers onto the substrate surface. In the following section we increase the size of the simulation cell further by employing a cube-on-cube methodology.

Cube-on-cube; MgO/CaO(001)

Following the 'cube-on-cube' methodology described above, the MgO/CaO(001) system was constructed by placing four layers of MgO on a CaO(001) substrate using a simulation cell size of 32×32 with the MgO constrained to occupy 'on-top' positions, thereby initially accommodating the entire -13% lattice misfit. The surface/interfacial area for the simulation cell is 5885 Å^2 and comprises 1024 atoms in each plane; an order of magnitude larger than the MgO/CaO system considered in the previous section using the atom deposition methodology. Dynamical simulation was applied to the system for 35 ps at 2000 K followed by energy minimisation.

In accord with the structures observed in the previous section, where the interface was constructed using the layer-by-layer deposition method, the present system also revealed the presence of large (up to *ca.* 9 Å) cracks within the MgO thin film (Fig. 5). However, inspection of the resulting structure suggests that the MgO structure may be better described as comprising small MgO clusters or islands on the substrate surface with inter-island separations of up to *ca.* 9 Å. The island sizes were calculated to be *ca.* 20×40, 40×40 and 70×20 Å in size. In addition, RDF values calculated for each

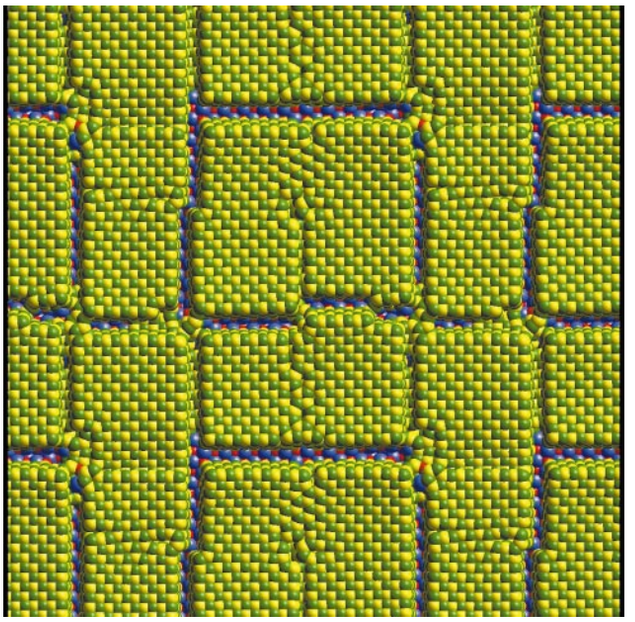

Fig. 5 Structure of the MgO/CaO(001) (32×32) interface after the deposition of four MgO layers onto the CaO support. Colour notation as Fig. 4.

MgO layer within the islands reveal average Mg–O distances of 2.05 (surface), 2.10, 2.15, 2.20 (interface) and 2.35 Å for the CaO interfacial plane, in accord with the values calculated in the previous section.

The formation of these islands is attributed to the lattice misfit between the two incommensurate materials. For example, whilst the initial 'on-top' configuration optimises the favourable cation–anion interactions across the interfacial plane, the strain energy associated with the MgO accommodating the entire −13% lattice misfit cannot be sustained. Accordingly, cracks appear within the MgO thin film resulting in small islands. At the interfacial plane, the MgO accommodates a lattice parameter close to the underlying CaO support to maximise the favourable interactions across the interface, while further from the interfacial plane, the MgO relaxes to its natural lattice parameter reducing the strain energy within the MgO lattice. It is envisaged that if further MgO species were deposited onto the surface of this thin film, the cracks would be 'filled', leading to an array of interfacial dislocations, evidence of which, was observed in the previous section, where the MgO/CaO(001) thin film was constructed using a layer-by-layer methodology. An experimental study by Dmowski *et al.* on the ceria/yttrium-stabilised zirconia interface constructed using vapour deposition of cerium followed by oxidative annealing suggests that the lattice constant mismatch between the ceria and zirconia is accommodated by the formations of islands which are orientationally matched to the substrate surface.[39]

For both the SrO/BaO(001) and MgO/CaO(001) interface systems, the supported SrO and MgO thin films relax back to their natural lattice parameter as one proceeds further from the interface resulting in cracks appearing at the surface of the thin films. In particular, for the SrO/BaO(001) system (−6.8% misfit) the cracks are relatively small (*ca.* 5 Å), whereas for the MgO/CaO(001) system, which is associated with a higher (−13%) lattice misfit, the cracks are as much as 9 Å. This study therefore demonstrates that the three methodologies reproduce qualitatively similar structural features. Moreover, the application of all three methodologies to a particular interface system can generate both structural information, associated with supporting a thin film on a substrate material (cube-on-cube), and its growth and nucleation mechanisms (atom deposition, layer-by-layer).

Systems with a positive misfit

We now explore the influence of interfaces associated with a large positive misfit. In particular we consider the SrO/MgO system, which is associated with a +20% lattice misfit. The main focus here is to elucidate the structural modifications that are associated with accommodating the lattice misfit. Accordingly, since the structural modifications may be large, we employ the cube-on-cube methodology to maximise the size of the simulation cell that can be addressed using the computational resources available. We first consider the SrO supported on MgO(001), which is the most stable MgO surface.

SrO/MgO(001)

The SrO/MgO(001) interface was constructed by placing four layers of SrO onto an MgO(001) substrate using a simulation cell size of 28×28 (3455 Å^2). The SrO was constrained to occupy 'on-top' positions thereby accommodating the entire +20% lattice misfit associated with this system. Dynamical simulation was then applied to the system for 150 ps at 2100 K followed by 90 ps at 1500 K, after which the system was energy minimised at 0 K and the resulting structure analysed.

The strain within the SrO associated with this initial configuration is considerable. Consequently, during the dynamical simulation, the Sr and O species move to alleviate the strain, generating an amorphous SrO thin film. Upon prolonged dynamical simulation, regions of the SrO start to recrystallise. In particular, Fig. 6 depicts the structure of the system after 25 ps and shows an SrO region, within the amorphous SrO, that is starting to recrystallise into a cubic structure. During prolonged dynamical simulation, the SrO thin film was observed to recrystallise completely, revealing a rocksalt structure.

For many simulations the starting configuration is likely to influence the final structure. Moreover, there is a danger, particularly within incommensurate interface systems, of generating structures, which may be artefacts of the initial configuration. Conversely, in this study, the SrO thin film recrystallised from an amorphous phase in which the SrO accommodated its natural lattice parameter, eliminating any possible influence or '*memory*' of the (strained) starting configuration.

Inspection of the final energy minimised structure reveals the presence of four dislocations within the SrO thin film,[24] one of which is presented in Fig. 7(a–c). The Burgers vector for this dislocation, which can be deduced most readily from inspection of Fig. 7(a), lies at *ca.* 45° to the line of the dislocation, which suggests that the dislocation has both screw and edge character.

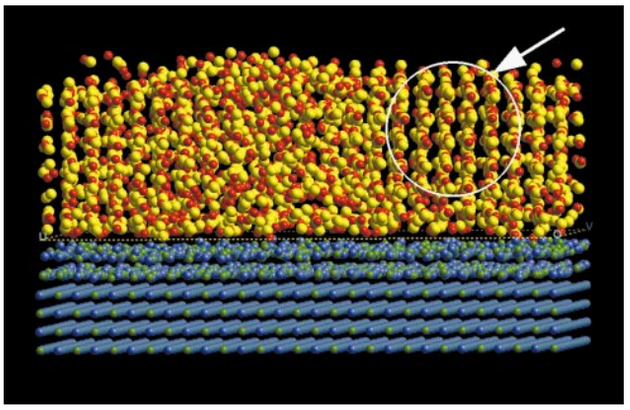

Fig. 6 Structure of the SrO/MgO(001) simulation cell after 25 ps of dynamical simulation depicting a region, encompassed by amorphous SrO, in which the SrO has started to recrystallise. Strontium is coloured yellow, magnesium is blue, oxygen (SrO) is red and oxygen (MgO) is green.

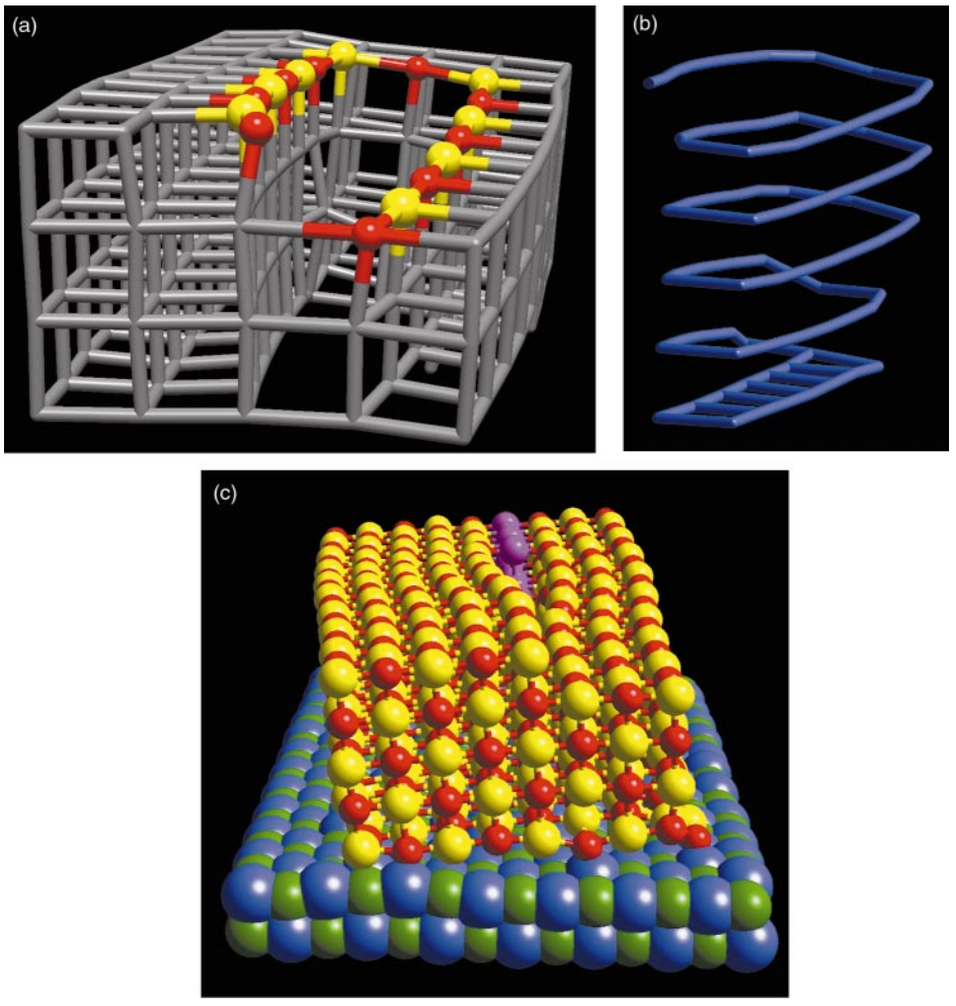

Fig. 7 Representations of the screw-edge dislocation within the SrO/MgO(001) interface: (a) depicts a section of the dislocation core within part of the surrounding SrO lattice (coloured grey); (b) Stick representation of the spiral of Sr and O atoms comprising the dislocation core; (c) representation of part of the SrO crystal, supported on the MgO substrate, depicting more clearly the edge component of the dislocation (atoms coloured purple). In addition, the figure demonstrates the low angle rotation of part of the SrO thin film with respect to the underlying MgO support.

Fig. 7(b) depicts more clearly the spiral of atoms comprising the core structure of the dislocation, whilst Fig. 7(c) shows the edge component (atoms coloured purple) of the dislocation.

We suggest that the combined screw-edge character arises in order to maintain charge continuity within this material of both positive and negative species: For a 'pure' screw dislocation, the core would have to spiral over 2 layers to maintain charge connectivity[23] and for a 'pure' edge dislocation, two MgO planes would have to be inserted. Accordingly, the screw component allows for the insertion of a single edge dislocation.

A stable interface is associated with unstrained thin film and support lattices in conjunction with optimised interfacial interactions. Clearly, for incommensurate systems such a configuration is not possible and a compromise must be sought.

RDF values, calculated for each SrO plane within the thin film, were found to be consistent with bulk SrO with no gradual change of cation–anion bond distance as a function of distance from the interface, in contrast to the interfaces considered in the previous section. Moreover, since the average cation–anion bond distances, for both the MgO and SrO, are equivalent to their 'bulk' values suggests also that there is little strain within the lattice. Inspection of the atom positions of the SrO with respect to the MgO support at the interfacial plane reveals that the Sr and O no longer accommodate positions directly on top of the underlying MgO, rather the SrO exists within particular 'domains', which lie either almost commensurate with the underlying MgO support or rotated at low angles. Dislocations are present at the domain boundaries within the SrO thin film facilitating the rotations. We tentatively suggest that the rotated domains quench lattice strain and enhance the interactions across the interfacial plane.

To determine the influence of the substrate surface on the structure of the supported thin film we consider two more systems: SrO/MgO(011) and SrO/MgO(14 0 1). The latter can be described as a stepped surface with an inter-step separation of *ca.* 30 Å.

SrO/MgO(011)

To generate the SrO/MgO(011) starting configuration, SrO(011) was placed onto a 3490 $Å^2$ MgO(011) substrate surface with the SrO constrained to accommodate an 'on-top' configuration. Dynamical simulation was then applied to the system for 143 ps at 2400 K followed by 85 ps at 1200 K, after which the system was energy minimised at 0 K and the resulting structure analysed. In accord with the SrO/MgO(001) system, during the initial stages of the dynamical simulation, the considerable strain within the SrO generates an amorphous SrO thin film structure, which recrystallises after further dynamical simulation.

The final structure (Fig. 8) reveals that the SrO exposes the (001) surface at the interface (Fig. 9). The system can therefore be characterised as SrO(001)/MgO(011) in contrast to the SrO(011)/MgO(011) starting configuration. In addition, the Sr and O species lie almost directly above the magnesium

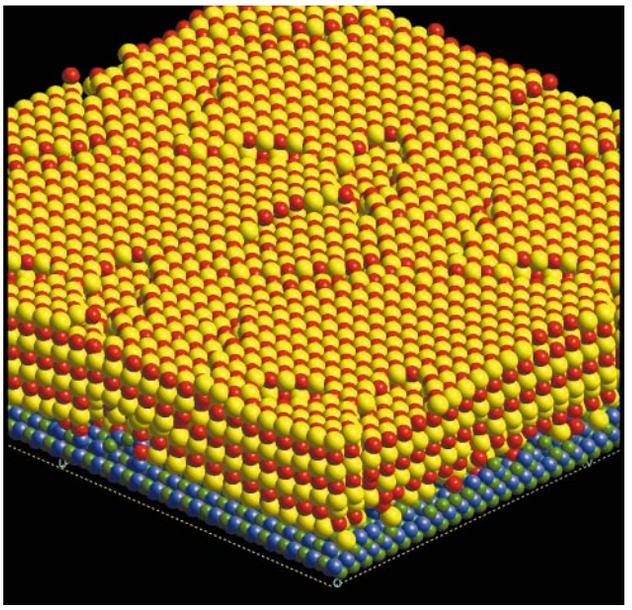

Fig. 8 Representation of the SrO/MgO(011) interface. Strontium is coloured yellow, magnesium is blue, oxygen (SrO) is red and oxygen (MgO) is green.

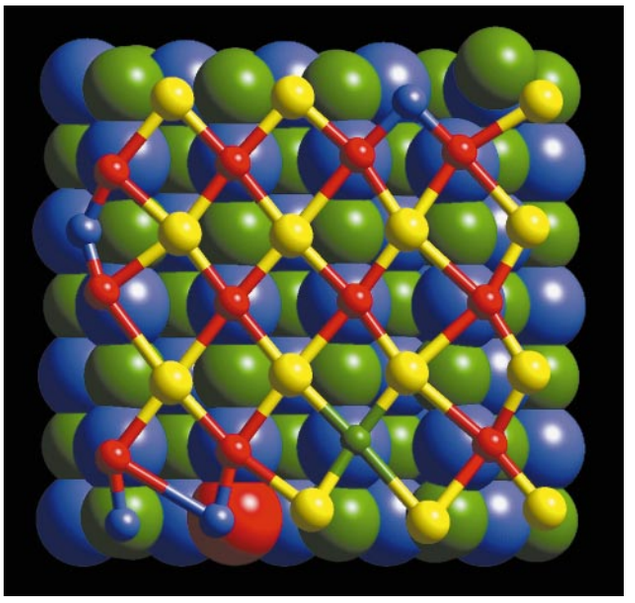

Fig. 9 Representation depicting part of the SrO/MgO(011) interface showing the interfacial SrO layer on top of the MgO(011) support with the Sr and O species lying almost directly above the magnesium sublattice of the MgO support. Colour notation as Fig. 8. Notice also the intermixing of ions across the interfacial planes; four magnesium ions (blue) occupy strontium lattice positions within the interfacial SrO layer and oxygen (green) from the underlying MgO has switched lattice positions with oxygen (red) from the SrO thin film (bottom of figure).

sublattice of the MgO(011) surface (Fig. 9). In particular, the oxygen ions (SrO) lie above the top layer of the magnesium sublattice of the MgO support, while the strontium ions lie above the second magnesium sublattice layer, bridging the oxygen ions in the top MgO(011) layer.

Close inspection of the surface of the SrO thin film (Fig. 8) revealed several screw-edge dislocations, one of which is presented in Fig. 10(a–c). Fig. 10(a) shows the spiral of Sr and O species within the dislocation core, while Fig. 10(b) depicts the dislocation core within part of the surrounding SrO lattice, demonstrating the long range influence of the dislocation on the surrounding SrO lattice. In particular, the SrO lattice planes [for example, within the white border of Fig. 10(b)], do not lie flat and parallel to the interfacial plane. Rather, they demonstrate considerable curvature in both the [100] and [010] directions. We also note that the curvature extends further than the region encompassed within the white border, although characterisation of the exact area over which the curvature extends proved difficult. It was observed, however, that the curvature extended to intersect other screw-edge dislocations, which eliminate the curvature, thus restoring the planarity of the SrO layer. The area over which the curvature extends was therefore estimated as 1100 $Å^2$, based upon the distances to neighbouring dislocations. To aid further the interpretation of the dislocation core, Fig. 10(c) depicts a side view of the interface, which includes both the SrO and the MgO support.

SrO/MgO(14 0 1)

To generate the SrO/MgO(14 0 1) starting configuration, SrO(14 0 1) was placed onto a 3464 $Å^2$ MgO (14 0 1) substrate surface with the SrO constrained to accommodate an 'on-top' configuration. Dynamical simulation was then applied to the system for 108 ps at 2300 K, followed by energy minimisation at 0 K. The resulting structure of the SrO thin film can be characterised as having a rocksalt-type structure. Steps on the surface of the supported SrO thin film are present. However, the steps follow an opposite direction compared with the MgO(14 0 1) support. A very loose analogy would be to compare the structure with that of a tilt grain boundary.[36,37] However, the thin film structure is rather more complex since the whole of the SrO (as opposed to particular domains as suggested in previous sections) is rotated with respect to the underlying MgO support by an angle of *ca.* 6° about an axis perpendicular to the interfacial plane. In addition, some of the steps arise from the formation of dislocations[33] within the SrO thin film, resulting in a perpendicular array of steps on the surface of the SrO. We now consider further the structure of the dislocations within the SrO thin film.

In accord with the previous two SrO/MgO interface systems, mixed screw-edge dislocations were observed within the SrO thin film and Fig. 11 depicts the core structure of three such dislocations. For two of the dislocations (coloured red and blue), the spiral of atoms traverses SrO lattice planes perpendicular to the interfacial plane in contrast to the third (coloured yellow), which lies parallel. Fig. 12 depicts a view, perpendicular to the interfacial plane, showing part of a single SrO plane and the dislocation core structure. Close inspection of this figure reveals two intersecting edge dislocations (coloured purple), which lie at 90° to each other.

Conclusion

We have seen how it is possible to use three methodologies for generating atomistic models of interfaces between incommensurate materials: 'Atom deposition' enables one to derive information on nucleation and growth mechanisms. 'Layer-by-layer' growth, which is computationally less expensive, enables one to address larger simulation cells, thereby limiting the problems associated with the periodic boundary conditions, whilst still generating information on the growth process and critical thicknesses. Finally, 'cube-on-cube', which involves only a single dynamical step, enables the investigation of considerably larger simulation cells. Consequently, misfit-induced structural modifications, which may be large, such as dislocations and low angle lattice rotations, can be explored. The study provides a framework on which to build and continue the study of supported thin films from small clusters to multilayer thin films, including their associated misfit-induced structural modifications.

In this study, simulation cell sizes of up to *ca.* 6000 $Å^2$ (interfacial surface area) have been considered. Previous studies on smaller systems have required that the thin film be

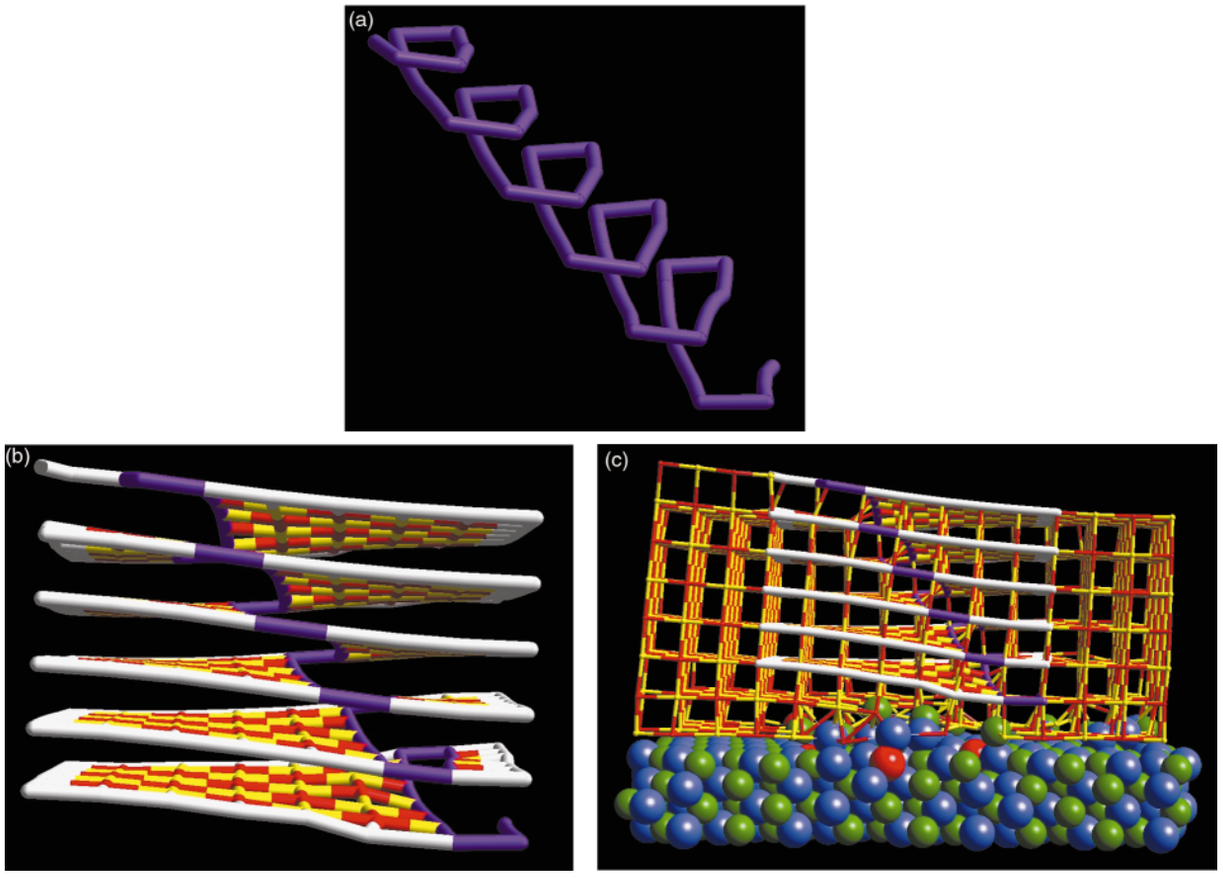

Fig. 10 Three representations of the screw-edge dislocation within the SrO/MgO(001) system are presented; (a) stick model representation of the spiral of Sr and O species (coloured purple) comprising the dislocation core within the SrO thin film lattice; (b) depicts the dislocation core within part of the surrounding SrO lattice, demonstrating the perturbation of the dislocation on the SrO lattice. To improve the clarity of the figure, the Sr and O ions at the outermost edges are coloured white; (c) here, more of the SrO lattice surrounding the dislocation core is presented, in addition to the MgO(011) support. Colour notation as Fig. 8. Notice also the intermixing of ions across the interfacial plane.

strained into coherency. Moreover, Schnitker and Srolovitz investigated the errors introduced into the work of adhesion associated with such assumptions of coherency and found they increased rapidly with misfit and can be "easily of the order of several tens of percent".[40] The authors attributed such errors to the neglect of the elastic fields associated with misfit dislocations and to the variation in the number of bonds per unit interfacial area with misfit when coherency is assumed. "Improved interface models must therefore account for the influence of dislocations within the lattice".[41] Calculations on the SrO/MgO interface, presented here, using much larger

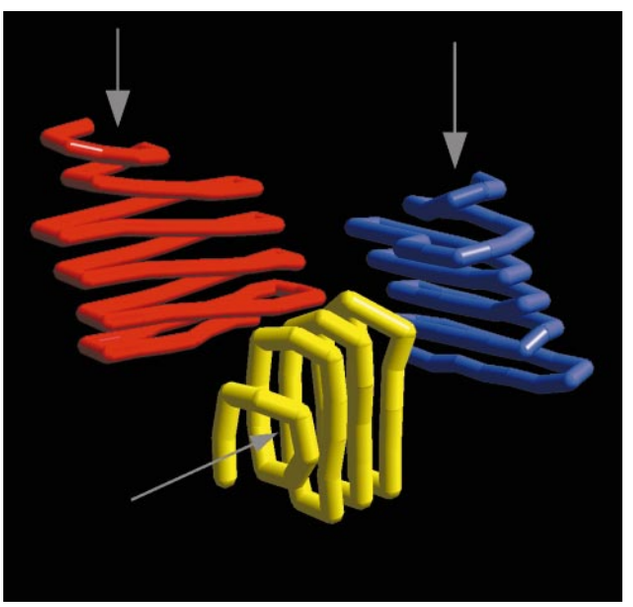

Fig. 11 Stick model representations of the spiral of Sr and O species comprising the dislocation cores of three screw edge dislocations within the SrO/MgO(14 0 1) system.

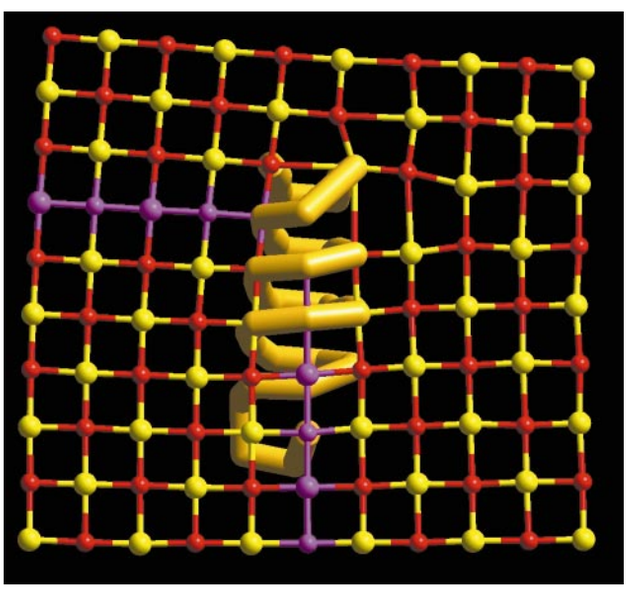

Fig. 12 Representation of a 'slice' cut parallel to the interfacial plane, through the SrO thin film lattice, depicting two edge dislocations lying at 90° to one another (coloured purple). The screw-edge dislocation (Fig. 11), coloured yellow, which lies parallel to the interfacial plane is also depicted.

simulation cells, have revealed the evolution of 'cracks', edge and screw dislocations, lattice slip, and low angle rotations of particular crystalline regions within the supported thin film, which address some of the inadequacies of previous models.

In summary, individually these techniques offer valuable information regarding the heteroepitaxial growth mechanisms and the role of dislocations in complex interfaces. Collectively these tools, as demonstrated by our results, offer a unique insight into the growth and structure of metal-oxide surfaces and interfaces, including critical thicknesses, which is, at present, difficult or indeed impossible to determine experimentally.

Future work will employ the methods developed in this study to explore supported catalysts, such as ceria supported on yttrium-stabilised zirconia. It is expected that for catalytic systems, the structural modifications at the surface of the thin film, arising as a consequence of the misfit-induced structural modifications, will influence the catalytic properties. In particular, it is apparent that the 'void' at the dislocation core is likely to provide a facile pathway for ions migrating from the bulk of the material to the surface of the thin film.

References

1 A. P. Sutton and R. W. Balluffi, *Interfaces in Crystalline Materials*, *Monographs on the physics and chemistry of materials*, vol. 51, Oxford University Press Inc., New York, 1995.
2 D. Wolf and J. A. Jaszczak, *J. Comput.-Aid. Mater. Des.*, 1993, **1**, 111.
3 G. Centi, S. Perathoner and F. Trifiro, *Res. Chem. Intermed.*, 1991, **15**, 49.
4 D. Dimos, P. Chaudhari and J. Mannhart, *Phys. Rev. B*, 1990, **41**, 4038.
5 S. Ramamurthy and C. B. Carter, *Phys. Status Solidi A*, 1998, **166**, 37.
6 R. A. McKee, F. J. Walker and M. F. Chisholm, *Phys. Rev. Lett.*, 1998, **81**, 3014.
7 N. D. Zakharov, D. Hesse, J. Auge, H. G. Roskos, H. Kurz, H. Hoffschulz, J. Dreßen, H. Stahl and G. Guntherodt, *J. Mater. Res.*, 1996, **11**, 2416.
8 F. Ernst, A. Recnik, P. A. Langjahr, P. D. Nellist and M. Ruhle, *Acta Mater.*, 1999, **47**, 183.
9 A. M. Stoneham, M. M. D. Ramos and A. P. Sutton, *Philos. Mag. A*, 1993, **67**, 797.
10 M. Kubo, Y. Oumi, R. Miura, A. Stirling, A. Miyamoto, M. Kawasaki, M. Yoshimoto and H. Koinuma, *Phys. Rev. B*, 1997, **56**, 13535.
11 D. C. Sayle, *J. Mater. Chem.*, 1999, **9**, 607.
12 A. L. Shluger, A. L. Rohl and D. H. Gay, *Phys. Rev. B*, 1995, **51**, 13631; A. L. Shluger, A. L. Rohl and D. H. Gay, *J. Vac. Sci. Technol. B*, 1995, **13**, 1190.
13 A. D. Novaco and J. P. McTague, *Phys. Rev. Lett.*, 1977, **38**, 1286.
14 P. W. Tasker and A. M. Stoneham, *J. Chim. Phys.*, 1987, **84**, 149.
15 R. W. Balluffi, A. Brokman and A. H. King, *Acta Metall.*, 1982, **30**, 1453.
16 A. P. Sutton and R. W. Balluffi, *Acta Metall.*, 1987, **35**, 2177.
17 T. X. T. Sayle, C. R. A. Catlow, D. C. Sayle, S. C. Parker and J. H. Harding, *Philos. Mag. A*, 1993, **68**, 565.
18 D. C. Sayle, A. S. Maicaneanu, B. Slater and C. R. A. Catlow, *J. Mater. Chem.*, 1999, **9**, 2779.
19 A. Valladares, J. A. White and A. P. Sutton, *Phys. Rev. Lett.*, 1998, **81**, 4903.
20 A. Valladares, A. K. Petford-Long and A. P. Sutton, *Philos. Mag. Lett.*, 1999, **79**, 9.
21 D. M. Duffy, *J. Phys. C: Solid State Phys.*, 1986, **19**, 4393.
22 G. W. Watson, E. T. Kelsey, N. H. de Leeuw, D. J. Harris and S. C. Parker, *J. Chem. Soc., Faraday Trans.*, 1996, **92**, 433.
23 G. W. Watson, E. T. Kelsey and S. C. Parker, *Philos. Mag. A*, 1999, **79**, 527.
24 D. C. Sayle, *J. Mater. Chem.*, 1999, **9**, 2961.
25 A. Serra, D. J. Bacon and R. C. Pond, *Acta Mater.*, 1999, **47**, 1425; R. C. Pond, A. Serra and D. J. Bacon, *Acta Mater.*, 1999, **47**, 1441.
26 L. Dong, J. Schnitker, R. W. Smith and D. J. Srolovitz, *J. Appl. Phys.*, 1998, **83**, 217.
27 D. C. Sayle, C. R. A. Catlow, M.-A. Perrin and P. Nortier, *J. Phys. Chem.*, 1996, **100**, 8940.
28 D. C. Sayle, T. X. T. Sayle, S. C. Parker, J. H. Harding and C. R. A. Catlow, *Surf. Sci.*, 1995, **334**, 170.
29 D. H. Gay and A. L. Rohl, *J. Chem. Soc., Faraday Trans.*, 1995, **91**, 925.
30 G. V. Lewis and C. R. A. Catlow, *J. Phys. C: Solid State Phys.*, 1985, **18**, 1149.
31 D. M. Lind, S. D. Berry, G. Chern, H. Mathias and L. R. Testardi, *Phys. Rev. B*, 1992, **45**, 1838.
32 F. C. Frank and J. Van der Merwe, *Proc. R. Soc. (London) A*, 1949, **198**, 216.
33 G. Springholz, *Appl. Surf. Sci.*, 1997, **112**, 12.
34 C. P. Sun and R. W. Balluffi, *Philos. Mag. A*, 1982, **46**, 49.
35 C. P. Sun and R. W. Balluffi, *Philos. Mag. A*, 1982, **46**, 63.
36 D. J. Harris, G. W. Watson and S. C. Parker, *Philos. Mag. A*, 1996, **74**, 407.
37 J. H. Harding, D. J. Harris and S. C. Parker, *Phys. Rev. B*, 1999, **60**, 2720.
38 C. A. J. Fisher and H. Matsubara, *Comput. Mater. Sci.*, 1999, **14**, 177; C. A. J. Fisher and H. Matsubara, *J. Eur. Ceram. Soc.*, 1999, **19**, 703.
39 W. Dmowski, E. Mamontov, T. Egami, S. Putna and R. Gorte, *Physica B*, 1998, **248**, 95.
40 J. Schnitker and D. J. Srolovitz, *Modell. Simul. Mater. Sci. Eng.*, 1998, **6**, 153.
41 S. C. Jain, A. H. Harker and R. A. Cowley, *Philos. Mag. A*, 1997, **75**, 1461.